Thrombosis Research 233 (2024) 55–68

Contents lists available at ScienceDirect

Thrombosis Research

journal homepage: www.elsevier.com/locate/thromres

Full Length Article

Driver gene *KRAS* aggravates cancer-associated stroke outcomes

Haomin Yan [a], Tsutomu Sasaki [a,b,*], Yasufumi Gon [a], Kumiko Nishiyama [a], Hideaki Kanki [a], Hideki Mochizuki [a]

[a] Department of Neurology, Graduate School of Medicine, Osaka University, Yamadaoka 2-2, Suita, Osaka 565-0871, Japan
[b] Department of Neurotherapeutics, Graduate School of Medicine, Osaka University, Osaka, Japan

ARTICLE INFO

Keywords:
Cancer-associated stroke
KRAS mutation
Neuroinflammation

ABSTRACT

The incidence of cancer-associated stroke has increased with the prolonged survival times of cancer patients. Recent genetic studies have led to progress in cancer therapeutics, but relationships between oncogenic mutations and stroke remain elusive. Here, we focused on the driver gene *KRAS*, which is the predominant RAS isoform mutated in multiple cancer types, in cancer associated stroke study. $KRAS^{G13D/-}$ and parental human colorectal carcinoma HCT116 cells were inoculated into mice that were then subjected to a photochemically-induced thrombosis model to establish ischemic stroke. We found that cancer inoculation exacerbated neurological deficits after stroke. Moreover, mice inoculated with $KRAS^{G13D/-}$ cells showed worse neurological deficits after stroke compared with mice inoculated with parental cells. Stroke promoted tumor growth, and the $KRAS^{G13D/-}$ allele enhanced this growth. Brain RNA sequencing analysis and serum ELISA showed that chemokines and cytokines mediating pro-inflammatory responses were upregulated in mice inoculated with $KRAS^{G13D/-}$ cells compared with those inoculated with parental cells. STAT3 phosphorylation was promoted following ischemic stroke in the $KRAS^{G13D/-}$ group compared with in the parental group, and STAT3 inhibition significantly ameliorated stroke outcomes by mitigating microglia/macrophage polarization. Finally, we compared the prognosis and mortality of colorectal cancer patients with or without stroke onset between 1 January 2007 and 31 December 2020 using a hospital-based cancer registry and found that colorectal cancer patients with stroke onset within 3 months after cancer diagnosis had a worse prognosis. Our work suggests an interplay between *KRAS* and ischemic stroke that may offer insight into future treatments for cancer-associated stroke.

1. Introduction

Currently one-in-ten patients with ischemic stroke are suffering comorbid cancer and the numbers are expected to increase in parallel with improvements in cancer therapies and the prolonging of survival rates [1]. Cancer-related procoagulants, inflammatory cytokines, and chemokines lead to the frequent occurrence of thrombosis in cancer patients [2,3] and are associated with subsequent cerebrovascular events and severe morbidity and mortality [4]. According to an autopsy study of patients with malignant cancers, approximately 7.4 % of patients showed clinical symptoms, while 14.6 % had pathologic evidence of stroke [5]. Cerebrovascular diseases occur frequently in cancer patients [6–8], among which colorectal cancer is a frequent malignant complication [9,10]. The accumulation of cerebrovascular risk factors throughout the lifetime of cancer patients makes cancer-associated stroke treatment urgent [11,12].

Our previous clinical studies demonstrated that cancer survivors [13], especially colorectal and pancreatic cancer patients [14], have a high risk of fatal ischemic stroke. Ischemic stroke patients with cancer showed worsened neurological deficits compared with ischemic stroke patients without cancer [15], and stroke occurrence can be predicted by a high neutrophil/lymphocyte ratio at cancer diagnosis [16]. We also observed that there was increased risk presumably due to cancer itself and not associated with chemotherapy use [17]. Nevertheless, the underlying mechanisms between cancer and stroke remain elusive. As reported in previous studies, approximately 17.4 % of cancer patients harbor *KRAS* mutations [18]. Additionally, the $KRAS^{G13D}$ allele accounts for approximately 20 % of all *KRAS* variants in colorectal cancer [19]. Thus, in this study, we focused on the effects of $KRAS^{G13D}$ on cancer-associated stroke.

* Corresponding author at: Department of Neurology, Graduate School of Medicine, Osaka University, Yamadaoka 2-2, Suita, Osaka 565-0871, Japan.
E-mail address: sasaki@neurol.med.osaka-u.ac.jp (T. Sasaki).

https://doi.org/10.1016/j.thromres.2023.11.015
Received 1 June 2023; Received in revised form 4 November 2023; Accepted 14 November 2023
Available online 19 November 2023

Signal transducer and activator of transcription 3 (STAT3) is known to be an oncogenic factor in KRAS-driven cancers [20,21]. Targeting STAT3 could be therapeutic in various cancers [22–24]. Accumulative studies also suggest an essential role for STAT3 in central nervous system diseases [25,26]. STAT3 has proinflammatory roles in central nervous system diseases by modulating microglial responses [27] and astrocyte activation [28]. Recent studies have reported that targeting STAT3 ameliorated post-stroke neuroinflammation [29]. However, the roles of STAT3 in cancer-associated stroke remain unclear.

In this study, we investigated the role of oncogenic *KRAS* in cancer-associated stroke using mice inoculated with $KRAS^{G13D/-}$ and wild-type (parental) HCT116 human colorectal cancer cells. We examined serum and brain levels of cytokines and chemokines after stroke in cancer-bearing mice, and then focused on STAT3-mediated neuroinflammation after stroke. We also compared the prognosis of colorectal cancer patients with or without a stroke development between 1 January 2007 and 31 December 2020.

2. Methods

2.1. Study approval

The Ethics Committee for Clinical Research at Osaka University Hospital approved this study. The need for informed consent was waived owing to the retrospective nature of the study. The whole animal experimental protocol was approved by the Institutional Animal Care and Use Committee of Osaka University Graduate School of Medicine.

2.2. Animals

Briefly, 7-week-old male C57BL/6 mice were purchased from Charles River Laboratories Japan (Yokohama, Japan) and randomly divided into each group. Mice were raised under standard conditions of light (12 h light/dark cycle) and temperature (23 °C, 40 % humidity).

2.3. Tumor cell inoculation

$KRAS^{G13D/-}$ HCT116 human colon cancer cells and parental HCT116 human colon cancer cells were purchased from Horizon Discovery (Waterbeach, UK). $KRAS^{G13D/-}$ HCT116 cancer cells were cultured in 10-cm dishes containing 10 % fetal bovine serum (Invitrogen, Carlsbad, CA, USA), 1 % antibiotic-antimycotic (Invitrogen), and 0.4 mg/mL G418 (Invitrogen) in RPMI1640. Parental HCT116 cancer cells were cultured in 10-cm dishes containing 10 % fetal bovine serum and 1 % antibiotic-antimycotic in RPMI1640. Cells (1×10^7 cells) were collected in 200 μL RPMI1640 and then subcutaneously injected into the backs of 7-week-old mice. Mice with subcutaneously injection of 200 μL RPMI1640 without cells were defined as the vehicle group. Tumors were isolated from skin using scissors and photographed with a digital microscope (SZX12, Olympus, Tokyo, Japan).

2.4. Drug administration

AG490 (Tokyo Chemical Industry, Tokyo, Japan) was dissolved in 0.3 % Dimethyl sulfoxide (DMSO) in saline according to the manufacturer's instruction for intraperitoneal injection of 3 mg/kg every other day from 7 d before to 7 d after surgery [30]. The weights of all mice were recorded once every day over the whole study.

2.5. Photochemically-induced thrombosis (PIT) model

Mice were subjected to PIT 14 d after cancer inoculation. Briefly, mice were rapidly anesthetized using 3.5 % isoflurane and maintained with 1.0 % isoflurane using an open mask. The skin along the midline of the scalp, from the eye level to the neck, was incised and the skull was exposed. Then, 5 min after intraperitoneal injection of 0.2 mL rose bengal (10 mg/mL), photothrombotic vascular occlusion was induced by 20 min of illumination applied to the right exposed skull using a cold light source (4.5 mm diameter fiber optic end; Hamamatsu Photonics K. K., Japan) placed 2.2-mm lateral (left) of the bregma. The illuminated area included the motor (M1) and somatosensory (S1) cortices. Mice with only skull mechanically exposure but without photochemically-induced thrombosis were defined as the sham group. After illumination, the skin of the scalp was closed. Mice were returned to their cages to recover separately.

2.6. Measurement of infarct volume

2,3,5-Triphenyltetrazolium chloride (TTC) staining was used to evaluate infarct volume as previously described [31].

2.7. Western blot

Ipsilateral and contralateral hemispheres of the mice were collected on days 1 and 14 after PIT. Proteins were extracted using lysis buffer (20 mM Tri-HCl, 150 mM NaCl, 2 mM EDTA, 1 % Nonidet P-40, protease inhibitor cocktail [Roche, Basel, Switzerland], and phosphatase inhibitor cocktail [Roche]). Protein concentrations were quantified using the BCA Protein Assay Kit (Thermo Fisher Scientific, Waltham, MA, USA). Next, 10 μg of protein lysate from each sample was subjected to electrophoresis and then transferred to a polyvinylidene difluoride membrane (Immobilon P; Millipore, Burlington, MA, USA). After 1 h of blocking with 5 % non-fat dry milk, membranes were incubated with primary antibody overnight at 4 °C. After 1 h of incubation with secondary antibody at room temperature, visualization was conducted with a luminoimage analyzer (ChemiDoc Touch MP, Bio-Rad, Hercules, CA, USA). The following antibodies were used: phospho-STAT3 (Tyr705) (1:1000; Cell Signaling Technology, Danvers, MA, USA), STAT3 (1:1000; Cell Signaling Technology), phospho-MEK1/2 (Ser221) (1:1000; Cell Signaling Technology), MEK1/2 (1:1000, Santa Cruz Biotechnology, Dallas, TX, USA), phospho-ERK1/2 (Thr202/Tyr204) (1:1000; Cell Signaling Technology), ERK1/2 (1:1000; Cell Signaling Technology), and β-actin (1:5000; Proteintech, Rosemont, IL, USA). Image J (Version 15.4 g18) was used for grey value quantification. For p-STAT3/STAT3, p-MEK/MEK and p-ERK/ERK calculation, after division by their individual relative expression value, the obtained ratios were normalized to the 1st left group for subsequent comparison, respectively.

2.8. Rotarod and foot fault tests

Rotarod and grid walking tests were used to evaluate neurological deficits as previously reported [32].

2.9. Enzyme-linked immunosorbent assay (ELISA)

Serum was collected from mice inoculated with parental or $KRAS^{G13D/-}$ HCT116 human colorectal cancer cells before and after PIT for ELISA with the Interleukin-6 Platinum (eBioscience, Vienna, Austria) and CXCL1/KC Quantikine (R&D Systems, Minneapolis, MN, USA) kits.

2.10. Quantitative real-time PCR (qPCR) analysis

Total RNA was extracted from brain tissues using the mirVana miRNA Isolation Kit (Thermo Fisher Scientific). cDNA was prepared from 1 μg total RNA using the SuperScript VILO cDNA Synthesis Kit (Invitrogen). Power SYBR Green PCR Master Mix (Thermo Fisher Scientific) was used for qPCR. Relative mRNA expression was calculated by the comparative CT method using the QuantStudio 7 Flex Real-Time PCR system (Applied Biosystems, Waltham, MA, USA). Gene expression levels were quantified by normalization to the expression of 36B4 as the endogenous control. The primer sequences used were as follows:

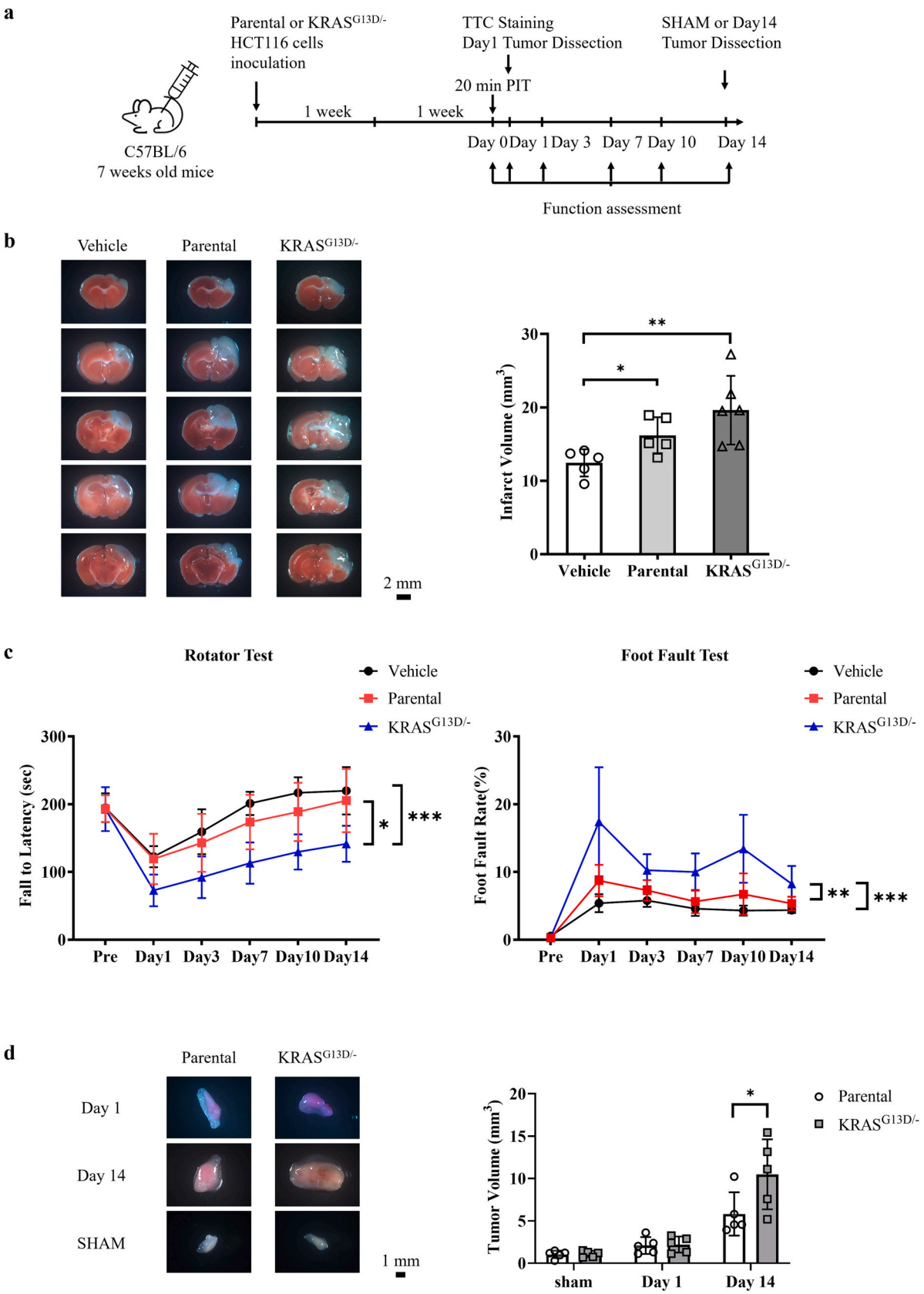

Fig. 1. Inoculation with *KRAS*$^{G13D/-}$ HCT116 cells aggravated experimental ischemic stroke outcomes without altering infarct volume. a. Mice were randomly divided into three groups and inoculated with RPMI1640 (vehicle), HCT116 human colorectal cancer cells (parental), or *KRAS*$^{G13D/-}$ HCT116 human colorectal cancer cells, and then subjected to photochemically-induced thrombosis (PIT) 2 weeks after inoculation. b. Representative images and measurements of tumors from the sham group 1 d after PIT and 14 d after PIT ($n = 5$–6). c. Rotarod and foot fault tests of mice in the vehicle, parental and *KRAS*$^{G13D/-}$ groups ($n = 5$ for vehicle

group, $n = 9$–10 for parental and $KRAS^{G13D/-}$ groups). d. Representative images and quantification of infarct volume in the vehicle, parental, and $KRAS^{G13D/-}$ groups (n = 5).

Ym-1 F: 5′-CAGGTCTGGCAATTCTTCTGAA-3′, R: 5′-GTCTTGCTCATGTGTGTAAGTGA-3′; Arginase-1 F: 5′-GGAATCTG-CATGGGCAACCTGTGT-3′, R: 5′-AGGGTCTACGTCTCGCAAGCCA-3′; TNFα F: 5′-GAGTGACAAGCCTGTAGCCCAC-3′, R: 5′-CTCAGCCCCCT-CAGGGGTGTC-3′; 36B4 F: 5′-TGTGTGTCTGCAGATCGGGT-3′, R: 5′-TGGATCAGCCAGGAAGGCCT-3′.

2.11. Immunofluorescence staining

Mice were sacrificed, and then perfused with ice-cold PBS followed by 2 % paraformaldehyde. Brains were isolated, postfixed in 2 % paraformaldehyde for 24 h, gradually dehydrated, and then cut into 14 μm-thick sections. Sections were incubated with 0.1 % TritonX-100 at room temperature for 30 min, and then incubated with 10 % donkey serum in PBS for 1 h. Slides were incubated with primary antibodies overnight at 4 °C, and then with secondary antibodies for 3 h at room temperature. Brain sections were counterstained with DAPI (Vector Laboratories, Burlingame, CA, USA). A confocal laser scanning microscope (FV3000, Olympus) was used for visualization. The following antibodies were used: CD16 (1:200; BD Biosciences, Franklin Lakes, NJ, USA), CD206 (1:200; R&D Systems), and Iba-1 (1:500; Wako, Osaka, Japan).

2.12. Analysis of RNA-seq data

RNA library preparation and sequencing were performed at the Center of Medical Innovation and Translation (CoMIT) Research Omics Center. RNA libraries were prepared for sequencing using the TruSeq Stranded mRNA Library Prep kit (Illumina, San Diego, CA, USA). Sequencing was performed on the Illumina Novaseq 6000 platform in the 100-bp paired-end mode. Fastq files were quality controlled using FastQC (0.11.7), and all samples passed quality control checks. After cleaning up adapter contamination and low-quality regions, reads were mapped to the GRCm38 (mm10) mouse genome reference using Hisat2 (2.1.0). Read counts were performed by featureCount (1.4.6). The R package DESeq2 (1.24.0) was used for count normalization and analysis of differentially expressed genes (DEGs) between 2 conditions. Heatmaps were generated using the R package pheatmap (1.0.12). Volcano plots were generated using the R package ggplot2 (3.4.0). Principle component analysis (PCA) was calculated by prcomp of R package stats (4.2.2) and visualized by R package ggplot2. Gene Ontology (GO) and Kyoto Encyclopedia of Genes and Genomes (KEGG) enrichment were conducted using R package clusterProfiler (4.6.0). The R package GOplot (1.0.2) was used to calculate Z scores, GO circular plots, and generate GO bubble plots. The Gene-Concept network was generated using R package enrichplot (1.18.3). KEGG enrichment was visualized by R package ggplot.

2.13. Patients and clinical variables

The retrospective study included 2933 patients who were newly diagnosed with colorectal cancer and admitted to Osaka University Hospital between 1 January 2007 and 31 December 2020. We included strokes that occurred after cancer diagnosis using a validated algorithm [33] to identify the occurrence of stroke during the follow-up period as previously reported [16,17,34]. Briefly, the algorithm indicated a stroke when the diagnostic code was registered and brain imaging (computed tomography and/or magnetic resonance imaging) was performed within a day of diagnosis. The diagnostic codes for stroke were based on the International Classification of Diseases (ICD)–10th revision as follows: subarachnoid hemorrhage (I60), intracerebral hemorrhage (I61), and cerebral infarction (I63). The algorithm had a 90 % positive predictive value for the clinical diagnosis of stroke.

We collected cancer-related information from the cancer registry including age, sex, cancer stage, initial anticancer treatment, and survival time. We also extracted clinical factors from electronic medical records including body mass index (BMI), smoking history, comorbidities (hypertension, dyslipidemia, diabetes mellitus, atrial fibrillation), use of antithrombotic medications, and blood biochemistry results at 1 month after cancer diagnosis (D-dimer, high sensitivity C-reactive protein [hsCRP], carcinoembryonic antigen [CEA], carbohydrate antigen 19-9 [CA19-9], and neutrophil/lymphocyte ratio [NLR]). Antithrombotic medications were defined as antiplatelet drugs (aspirin, cilostazol, ticlopidine, and clopidogrel) and anticoagulant agents (warfarin, dabigatran, edoxaban, apixaban, and rivaroxaban). As our cancer registry only included initial cancer treatment, we extracted data on all cancer treatments performed during the study period. ICD–10 codes were used to define the following comorbidities: hypertension (I20–I25), dyslipidemia (E78), diabetes mellitus (E10–E14), and atrial fibrillation (E48).

2.14. Follow-up

The observation period was from 1 January 2007 to 31 December 2022. The index date was defined as the date of cancer diagnosis or the date of the patient's first visit to Osaka University Hospital (for patients referred after diagnosis). The end date of follow-up was the time of death, last visit to our hospital, or 5 years after cancer diagnosis.

2.15. Statistical analysis

GraphPad Prism (v9.3.1; GraphPad Software, Inc., San Diego, CA, USA) was used to analyze the data from animal experiments. Comparisons between two separate groups were performed using the unpaired non-parametric *t*-test. Multiple group comparisons were performed using one-way ANOVA with Bonferroni's post hoc test. Data from rotarod and foot fault tests were compared with repeated measurement 2-way ANOVA. A two-tailed *P*-value <0.05 was considered statistically significant. All data are presented as mean ± standard deviation (SD).

For patient data, continuous variables are presented as median (interquartile range [IQR]) and categorial variables are described as count (percentage). Values were compared using the Mann–Whitney *U* test and chi-square test as appropriate. Patients were divided into two groups according to stroke occurrence after cancer diagnosis, and then baseline characteristics were compared between the groups. To examine the specific effect of stroke on the survival of cancer patients, we applied landmark analysis in accordance with stroke status using three timepoints. Statistical analysis was performed using R (4.2.2). All tests were two-tailed. The level of significance was set at $P < 0.05$.

3. Results

3.1. $KRAS^{G13D/-}$-driven cancer and stroke mutually aggravated each other

To examine the roles of oncogenic *KRAS* in cancer-associated stroke, mice were randomly divided into three groups and inoculated with RPMI1640 (vehicle), HCT116 human colorectal cancer cells (parental), or $KRAS^{G13D/-}$ HCT116 human colorectal cancer cells, and then subjected to 20 min PIT on day 14 after inoculation (Fig. 1a). Infarct volumes were significantly increased in both mice inoculated with parental and $KRAS^{G13D/-}$ HCT116 cells compared with the vehicle group (Fig. 1b). Neurological tests from day 1 up to day 14 after stroke revealed that neurological deficits were significantly worsened in the $KRAS^{G13D/-}$ group compared with the parental HCT116 group by

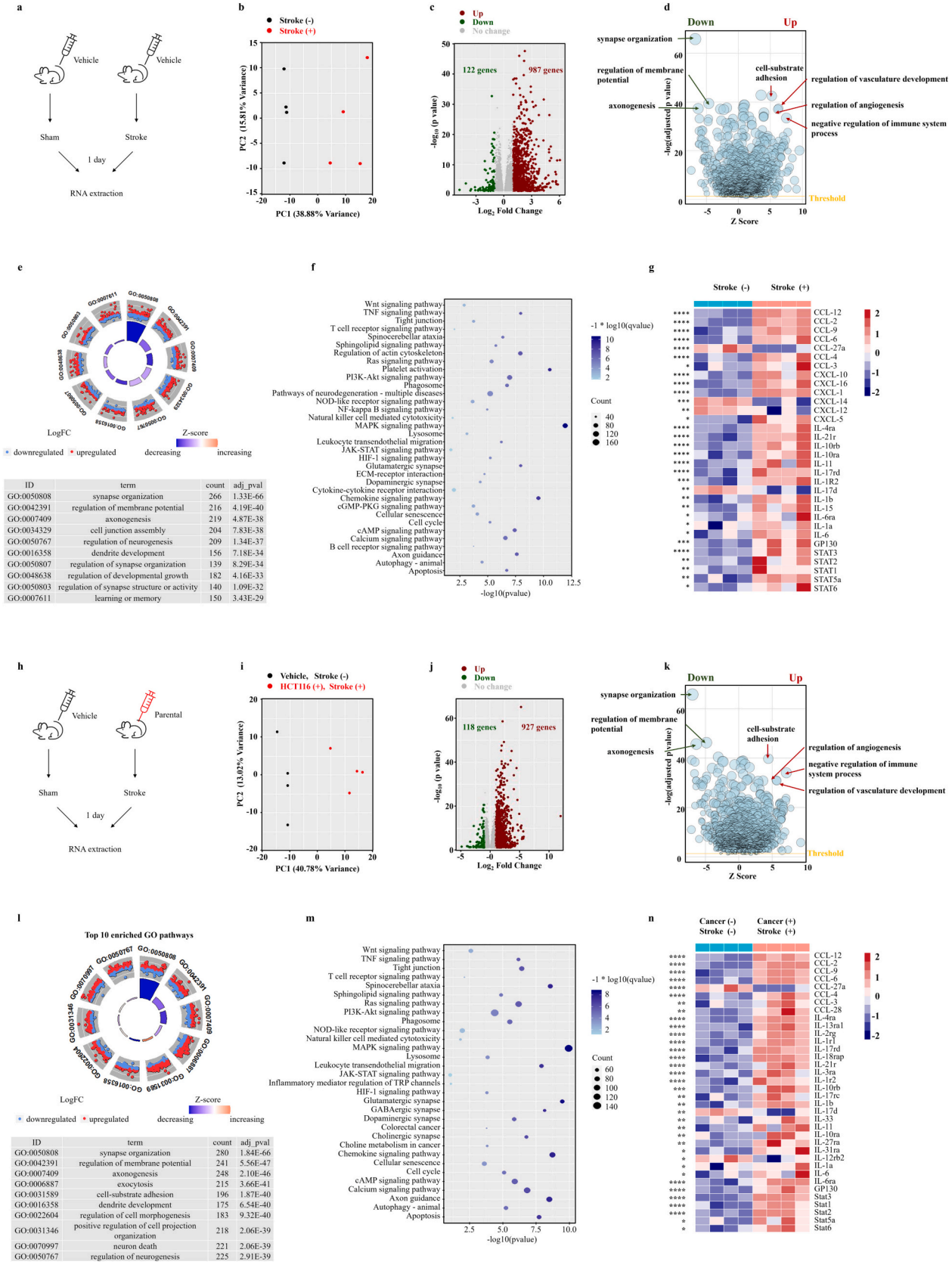

ID	term	count	adj_pval
GO:0050808	synapse organization	266	1.33E-66
GO:0042391	regulation of membrane potential	216	4.19E-40
GO:0007409	axonogenesis	219	4.87E-38
GO:0034329	cell junction assembly	204	7.83E-38
GO:0050767	regulation of neurogenesis	209	1.34E-37
GO:0016358	dendrite development	156	7.18E-34
GO:0050807	regulation of synapse organization	139	8.29E-34
GO:0048638	regulation of developmental growth	182	4.16E-33
GO:0050803	regulation of synapse structure or activity	140	1.09E-32
GO:0007611	learning or memory	150	3.43E-29

ID	term	count	adj_pval
GO:0050808	synapse organization	280	1.84E-66
GO:0042391	regulation of membrane potential	241	5.56E-47
GO:0007409	axonogenesis	248	2.10E-46
GO:0006887	exocytosis	215	3.66E-41
GO:0031589	cell-substrate adhesion	196	1.87E-40
GO:0016358	dendrite development	175	6.54E-40
GO:0022604	regulation of cell morphogenesis	183	9.32E-40
GO:0031346	positive regulation of cell projection organization	218	2.06E-39
GO:0070997	neuron death	221	2.06E-39
GO:0050767	regulation of neurogenesis	225	2.91E-39

Fig. 2. Transcriptome profiling of cancer bearing mice following stroke. a. Hemispheres isolated from sham and stroke mice on day 1 were used for RNA sequencing analysis ($n = 4$). b. Principal component analysis (PCA), c. volcano plot, and d. Gene ontology (GO), e. GO circular plot, f. Kyoto Encyclopedia of Genes and Genomes (KEGG) enrichment analysis, and g. heatmap for the two groups. h. Ipsilateral hemisphere isolated from cancer-bearing mice and sham hemisphere from mice without cancer were used for RNA sequencing analysis ($n = 4$). i. PCA, j. volcano plot, k. GO bubble plot, l. GO circular plot, m. Kyoto Encyclopedia of Genes and Genomes (KEGG) enrichment analysis, and n. heatmap for the two groups.

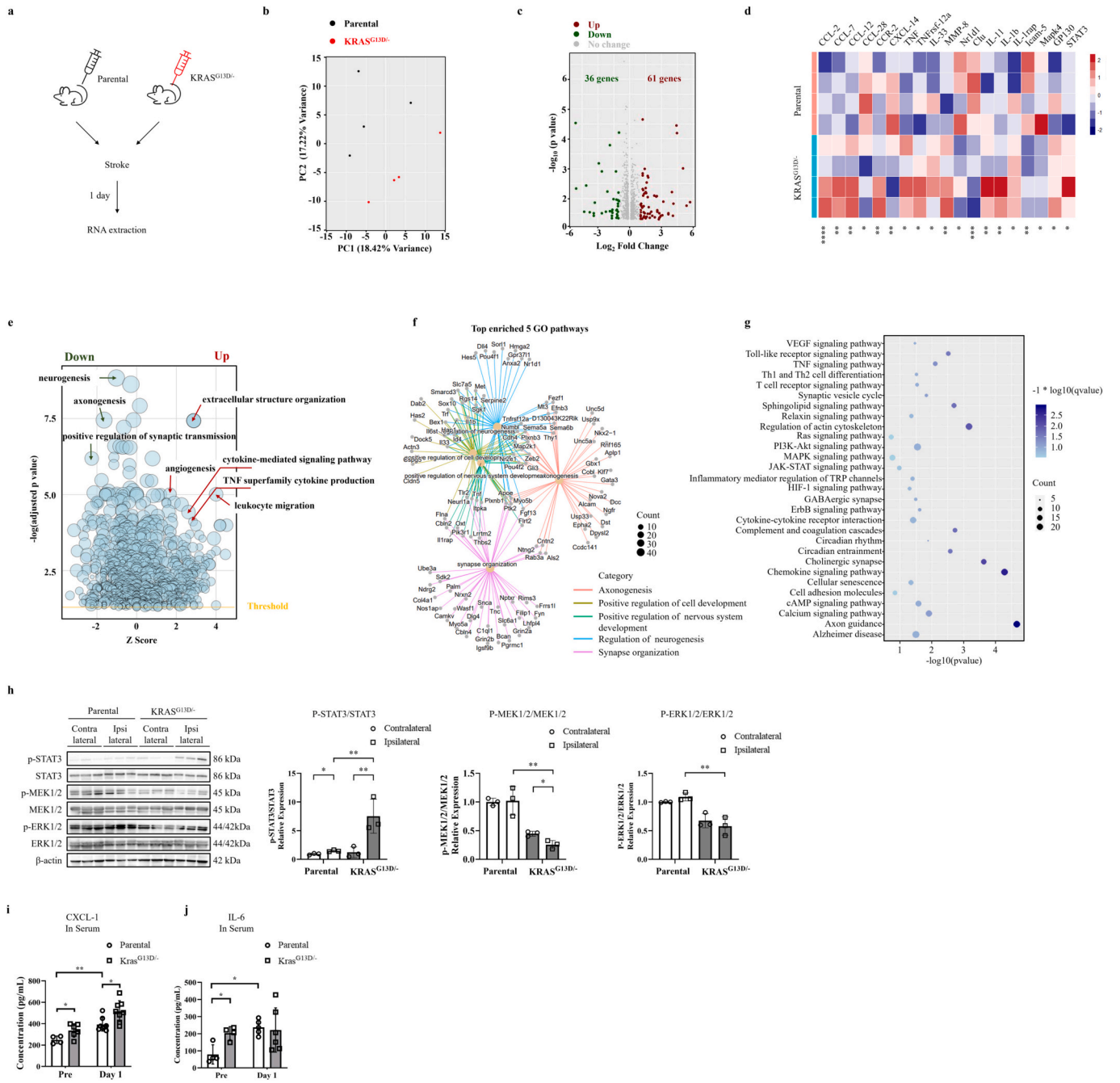

Fig. 3. *KRAS*$^{G13D/-}$-driven xenografts induced elevated chemokine and cytokine expression and STAT3 phosphorylation in the brain. a. Stroke hemispheres isolated from mice inoculated with parental and *KRAS*$^{G13D/-}$ HCT116 cells were applied for RNA sequencing analysis (n = 4). b. Principal component analysis (PCA), c. volcano plot, d. heatmap, e. Gene Ontology (GO) bubble plot, f. Gene-Concept network plot, and g. Kyoto Encyclopedia of Genes and Genomes (KEGG) enrichment analysis between stroke hemispheres of the parental and *KRAS*$^{G13D/-}$ groups. h. Representative western blots and quantification of P-STAT3:STAT3, P-MEK1/2:MEK1/2, and P-ERK1/2:ERK1/2 levels in contralateral and ipsilateral hemispheres of mice inoculated with parental and KRAS$^{G13D/-}$ HCT116 cells ($n = 3$). i. Serum CXCL1 concentration was measured by ELISA before and 1 d after photochemically-induced thrombosis (PIT) in the parental and *KRAS*$^{G13D/-}$ groups (n = 4–6 for pre, $n = 8$ for day 1). j. Serum IL-6 concentration was measured by ELISA before and 1 d after PIT in the parental and *KRAS*$^{G13D/-}$ groups (n = 4 for pre, n = 5–6 for day 1).

rotarod ($F(5, 108) = 2.351$, $p = 0.0456$) and foot fault ($F(5, 107) = 4.415$, $p = 0.0011$) tests (Fig. 1c). In comparison with the vehicle group, mice in the *KRAS*$^{G13D/-}$ group showed an enhanced worse neurological deficits by rotarod ($F(5, 78) = 4.735$, $p = 0.0008$) and foot fault test ($F(5, 78) = 4.695$, $p = 0.0008$). No statistically significant differences between the parental and vehicle group were observed, which might be due to the limited samples scale and effects of deviations in neurological tests. As previous reports have already demonstrated that tumor would enhance the worsened prognosis after stroke [35,36], further experiments including increase of animal numbers are needed to elucidate the interactions between parental HCT116 tumor and stroke. Additionally, tumor size expanded by approximately 2-fold 1 d after PIT and by approximately 5-fold 14 d after PIT in mice inoculated with parental HCT116 cells compared with the sham group, while *KRAS*$^{G13D/-}$ tumors grew by approximately 1.8-fold compared with parental HCT116 tumors 14 d after PIT (Fig. 1d), indicating that stroke accelerated tumor

growth, which was further enhanced by the $KRAS^{G13D/-}$ mutation. These results suggest that cancer and stroke mutually aggravated each other, with the $KRAS^{G13D/-}$ mutation enhancing both cancer growth and experimental stroke impairment.

3.2. Transcriptome profiling of cancer-bearing mice following stroke

First, we compared RNA transcriptome profiles of stroke and sham hemispheres from the mice (Fig. 2a). PCA revealed a clear difference in gene expression between the two groups (Fig. 2b). After stroke, 987 genes were upregulated and 122 genes were downregulated (Fig. 2c). GO enrichment analysis revealed that the DEGs were enriched in cell-substrate adhesion, negative regulation of immune system process, regulation of angiogenesis, regulation of vasculature development, synapse organization, regulation of membrane potential, and axonogenesis pathways (Fig. 2d). The top 10 GO pathways according to adjusted *P* values are listed in Fig. 2e. We also performed KEGG enrichment analysis to identify pathological pathways (Fig. 2f). The top three KEGG pathways according to adjusted P values were MAPK signaling pathway, platelet activation, and chemokine signaling pathway. Among all the DEGs, chemokines such as CCL-12, CCL-2, CCL-9, CCL-6, CCL-27a, CCL-4, CCL-3, CXCL-10, CXCL-16, CXCL-1, CXCL-14, CXCL-12, CXCL-5, and cytokines such as interleukins showed significant differences in the stroke hemisphere (Fig. 2g). Next, to evaluate molecular mechanisms of cancer-associated stroke, we compared the RNA transcriptome profiles of stroke hemispheres isolated from HCT116 cancer bearing mice and sham hemispheres from mice without cancer (Fig. 2h). PCA revealed a clear difference in gene expression between the two groups (Fig. 2i). Compared with sham hemispheres from mice in the vehicle group, there were 927 upregulated and 118 downregulated genes in stroke hemispheres from cancer-bearing mice (Fig. 2j). GO enrichment analysis revealed that DEGs of the stroke hemisphere from cancer-bearing mice were enriched in cell-substrate adhesion, negative regulation of immune system process, regulation of angiogenesis, regulation of vasculature development, synapse organization, regulation of membrane potential, and axonogenesis pathways (Fig. 2k). The top 10 GO pathways according to adjusted *P* values are listed in Fig. 2l. We also performed KEGG enrichment analysis to identify pathological pathways (Fig. 2m). The top three KEGG pathways according to adjusted P values were MAPK signaling pathway, glutamatergic synapse, and chemokine signaling pathway. Among all the DEGs, chemokines such as CCL-12, CCL-2, CCL-9, CCL-6, CCL-27a, CCL-4, CCL-3, CCL-28, and cytokines such as interleukins showed significant differences in the stroke hemispheres of cancer bearing mice (Fig. 2n). IL-6, IL-6ra, GP130, and STAT3 showed significant upregulation in the stroke hemisphere of cancer bearing mice, indicating activation of the IL-6/GP130/STAT3 pathway. To directly evaluate molecular mechanisms of cancer-associated stroke in brain, we compared the RNA transcriptome profiles of stroke hemispheres isolated from mice inoculated with parental HCT116 cancer and mice with vehicle (Supplemental Fig. 1a). PCA revealed a clear difference in gene expression between the two groups (Supplemental Fig. 1b). 30 genes were upregulated and 27 genes were downregulated in mice with HCT116 tumor in comparison with mice without tumor (Supplemental Fig. 1c). GO enrichment analysis revealed that the DEGs were enriched in collagen fibril organization, extracellular matrix organization, muscle organ development, muscle cell differentiation, stress-activated MAPK cascade (Supplemental Fig. 1d). The top 10 GO pathways according to adjusted *P* values are listed in Supplemental Fig. 1e. We also performed KEGG enrichment analysis to identify pathological pathways (Supplemental Fig. 1f). DEGs were significantly enriched in chemokines and cytokines, pathways of stress-activated MAPK cascade, regulation of vasculature development and platelet-derived growth factor binding (Supplemental Fig. 1g). STAT3 showed no significant difference between the two groups. The underlying regulatory mechanism of parental HCT116 tumor inoculation in stroke hemisphere deserves further researches.

3.3. $KRAS^{G13D/-}$-mutant cancer modulated chemokines and cytokines and induced STAT3 activation in the brain

To investigate the underlying molecular pathways between stroke in mice bearing parental and $KRAS^{G13D/-}$ HCT116 cells, we compared RNA transcriptome profiles of stroke hemispheres isolated from mice in these two groups (Fig. 3a). PCA revealed a clear difference in gene expression between the two groups (Fig. 3b). In the stroke hemispheres of mice inoculated with $KRAS^{G13D/-}$ cells, 61 genes were upregulated and 36 genes were downregulated (Fig. 3c). Chemokines such as CCL-2, CCL-7, CCL-12, CCL-28, CXCL-14, cytokines such as TNF, and interleukins showed significant differences in the stroke hemispheres from cancer bearing mice (Fig. 3d). Among the DEGs, TNF, IL-33, MMP-8, Nr1d1, and Clu indicated microglia cell activation (GO ID: 0001774). Additionally, GP130 and STAT3 showed enhanced upregulation in the stroke hemisphere of mice inoculated with $KRAS^{G13D/-}$ cells compared with parental HCT116 cells. GO enrichment analysis revealed that the DEGs were enriched in extracellular structure organization, cytokine-mediated signaling pathway, TNF superfamily cytokine production, leukocyte migration, angiogenesis, axonogenesis, and synaptic transmission pathways (Fig. 3e). The top five GO pathways (adjusted *P* value $<10^{-4}$) according to gene counts are included in the Gene-Concept network in Fig. 3f. KEGG enrichment analysis was also applied to identify pathological pathways following stroke in mice bearing $KRAS^{G13D/-}$ cancer (Fig. 3g). The top three KEGG enriched pathways according to adjusted *P* values were axon guidance, chemokine signaling, and cholinergic synapse.

We used western blot analysis to measure STAT3 and p44/42 MAPK activation in brain tissues of mice following stroke (Fig. 3h). On day 1 after PIT, STAT3 was significantly phosphorylated in the ischemic ipsilateral hemisphere, and $KRAS^{G13D/-}$ tumor inoculation significantly enhanced STAT3 phosphorylation in the ipsilateral hemispheres. Phosphorylation of both MEK1/2 and ERK1/2 was significantly decreased in mice inoculated with $KRAS^{G13D/-}$ HCT116 cells compared with mice inoculated with parental HCT116 cells. Next, we evaluated serum chemokine and cytokine levels in mice inoculated with parental and $KRAS^{G13D/-}$ cells. Tumors secrete CXCL1, which activates inflammation and aggravates prognosis in cancer-bearing mice [37]. Circulating CXCL1 has been found to be elevated in ischemic stroke patients and to promote inflammatory cell migration [38,39]. Consistent with previous studies, on day 1 after stroke, serum CXCL1 levels were significantly increased in both parental and $KRAS^{G13D/-}$ tumor-bearing mice, with the $KRAS^{G13D/-}$ mutation enhancing serum CXCL1 levels both before and after stroke (Fig. 3i). IL-6 plays crucial roles in both stroke [40] and tumor [41] outcomes. Before stroke, serum IL-6 concentrations were significantly elevated in the $KRAS^{G13D/-}$ group compared with the parental HCT116 group (Fig. 3j). After stroke, serum IL-6 levels were significantly increased in the parental HCT116 group. Further studies are needed to elucidate the dynamics of CXCL-1 and IL-6 in serum and brain. These results suggest that $KRAS^{G13D/-}$-mutant cells could modulate chemokines and cytokines and enhance STAT3 activation in the brains of tumor-bearing mice.

3.4. STAT3 inhibition ameliorated stroke outcomes in mice inoculated with $KRAS^{G13D/-}$ cells

To clarify the role of STAT3 activation in stroke of mice inoculated with $KRAS^{G13D/-}$ cancer, we administrated AG490, a selective STAT3 inhibitor every other day to cancer-bearing mice from 7 days before stroke to 7 days after stroke (Fig. 4a). Weights of mice in each group were recorded daily, and there were no statistical differences in weight gain among the groups during the study (Supplemental Fig. 2). We examined STAT3 activation in ipsilateral hemispheres after ischemic stroke by western blot on day 1 (Fig. 4b) and 14 (Fig. 4c) after stroke. Compared with the parental + DMSO group, the $KRAS^{G13D/-}$ + DMSO group showed significantly elevated pSTAT3 activation, while AG490

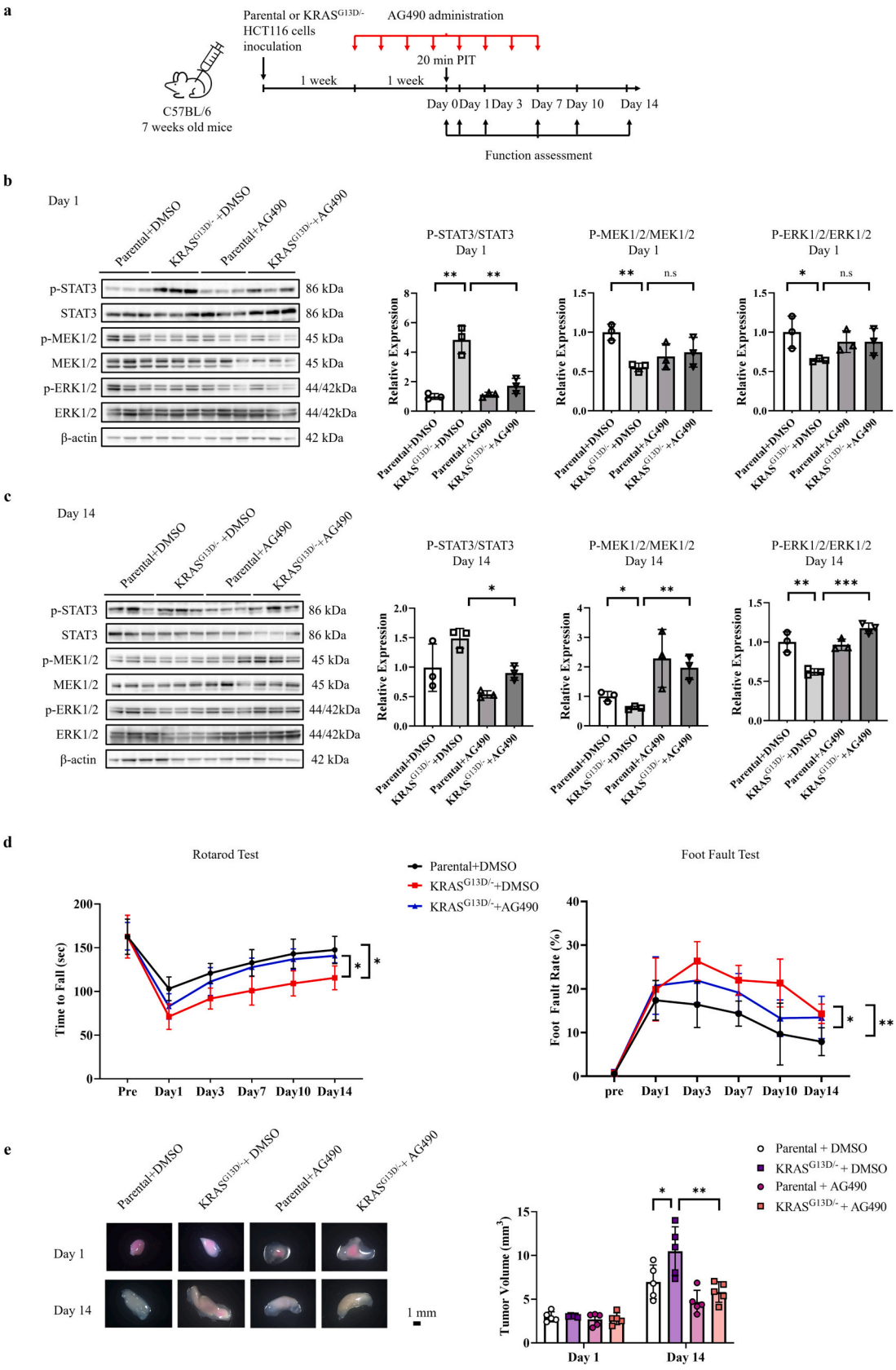

Fig. 4. AG490 ameliorated ischemic stroke outcomes by inhibiting STAT3 activation and attenuating MEK1/2 and ERK1/2 inhibition. a. AG490 was used as a selective STAT3 inhibitor and was intraperitoneally injected into cancer bearing mice every other day from 7 d before photochemically-induced thrombosis (PIT) to 7 d after PIT. b-c. Representative western blots and quantification of P-STAT3:STAT3, P-MEK1/2:MEK1/2, and P-ERK1/2:ERK1/2 levels in the ipsilateral hemispheres of mice in the parental and *KRAS*$^{G13D/-}$ groups on b. day 1 and c. day 14 after PIT ($n = 3$). d. Rotarod and foot fault tests of mice in the parental and *KRAS*$^{G13D/-}$ groups ($n = 9$). e. Representative images and measurements of tumor size on days 1 and 14 after ischemic stroke (n = 5).

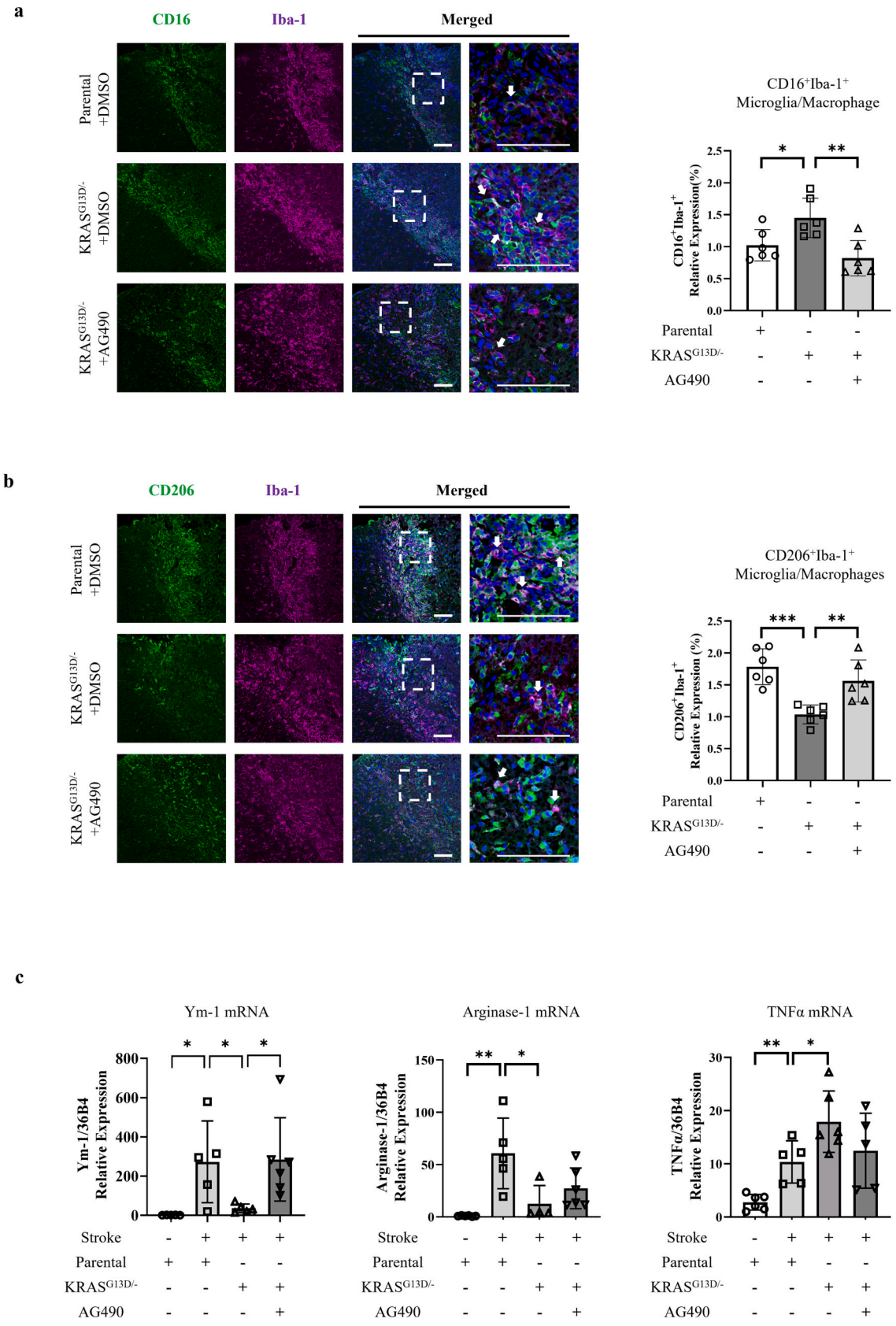

Fig. 5. AG490 modulated macrophage/microglia polarization in the ipsilateral hemisphere and repressed proinflammatory responses. a. Representative immunostaining images and quantification of $CD16^{+}Iba\text{-}1^{+}$ M1-like microglia/macrophages in the ipsilateral hemisphere of mice on day 7 after photochemically-induced thrombosis (PIT); scale bar = 100 μm. b. Representative immunostaining images and quantification of $CD206^{+}Iba\text{-}1^{+}$ M2-like microglia/macrophages in the ipsilateral hemisphere of mice on day 7 after PIT. Quantification was performed using six sections from three individual mice from each group. c. qPCR results of Ym-1, Arginase-1, and TNFα mRNA levels in the ipsilateral hemisphere of mice on day 1 after stroke (n = 5–6).

administration significantly suppressed the phosphorylation, both on day 1 and 14 after stroke. We also evaluated p44/42 MAPK activation. AG490 significantly attenuated MEK1/2 and ERK1/2 inhibition in the $KRAS^{G13D/-}$ group on day 14 after stroke.

Next, to evaluate whether STAT3 is associated with the impaired neurological deficits induced by oncogenic $KRAS^{G13D/-}$-mutant tumor inoculation, rotarod and foot fault tests were conducted among parental + DMSO, $KRAS^{G13D/-}$ + DMSO and $KRAS^{G13D/-}$ + AG490 groups before and 1, 3, 7, 10, 14 d after stroke (Fig. 4d). The $KRAS^{G13D/-}$ group showed worse neurological recovery compared with the parental group in both rotarod ($KRAS^{G13D/-}$ + DMSO vs. parental + DMSO: $F(5, 96) = 3.097$, $p = 0.0148$) and foot fault ($KRAS^{G13D/-}$ + DMSO vs. parental + DMSO: $F(5, 96) = 4.441$, $p = 0.0011$) tests. AG490 administration significantly attenuated the effects of $KRAS^{G13D/-}$ tumors in both rotarod ($KRAS^{G13D/-}$ + AG490 vs. $KRAS^{G13D/-}$ + DMSO: $F(5, 96) = 2.327$, $p = 0.0485$) and foot fault ($KRAS^{G13D/-}$ + AG490 vs. $KRAS^{G13D/-}$ + DMSO: $F(5, 96) = 2.395$, $p = 0.0430$) tests. AG490 also significantly suppressed the growth of $KRAS^{G13D/-}$-mutant cancer on day 14 after stroke (Fig. 4e). These data indicate that AG490 significantly attenuated the outcomes of stroke in mice inoculated with $KRAS^{G13D/-}$ cancer by inhibiting STAT3 activation and attenuating MEK1/2/ERK1/2 inhibition in the brain and suppressing tumor growth.

3.5. STAT3 inhibition modulated macrophage/microglia polarization and repressed neuroinflammation after stroke

Microglia/macrophage polarization could either exacerbate neuronal damage or promote neural repair after ischemic stroke. Previous studies have reported that the number of neuroprotective M2-like microglia/macrophages accelerates to a maximum on day 7 after ischemic stroke [30,42]. To evaluate microglia/macrophage polarization in the ipsilateral hemisphere, we conducted CD16 (M1-like microglia/macrophage marker)/Iba-1 (microglia/macrophage marker), and CD206 (M2-like microglia/macrophage marker)/Iba-1 immunofluorescence staining of brain sections from mice on day 7 after stroke (Fig. 5a and b). Both M1-like microglia/macrophages ($CD16^{+}Iba\text{-}1^{+}$ cells) and M2-like microglia/macrophages ($CD206^{+}Iba\text{-}1^{+}$ cells) accumulated in the peri-infarct area, while in mice inoculated with $KRAS^{G13D/-}$ cells, there were significantly more M1-like microglia/macrophages ($CD16^{+}Iba\text{-}1^{+}$ cells) and less M2-like microglia/macrophages ($CD206^{+}Iba\text{-}1^{+}$ cells) in the peri-infarct brain area. AG490 significantly suppressed the elevation in M1-like microglia/macrophages ($CD16^{+}Iba\text{-}1^{+}$ cells) and attenuated the decrease in M2-like microglia/macrophages ($CD206^{+}Iba\text{-}1^{+}$ cells) in the peri-infarct area of mice in the $KRAS^{G13D/-}$ group.

In the acute ischemic stroke phase, M1-like microglia/macrophages secrete proinflammatory cytokines such as TNF, while M2-like microglia/macrophages produce cytokines such as Arginase-1 and Ym-1 [43]. We conducted qPCR to evaluate Ym-1, Arginase-1, and TNFα expression in the ipsilateral hemisphere. Compared with the sham group, mice subjected to stroke showed higher Ym-1, Arginase-1, and TNFα mRNA levels in the ipsilateral hemisphere, especially in the acute stroke phase (day 1 after stroke) (Fig. 5c). Mice in the $KRAS^{G13D/-}$ group showed decreased Arginase-1 and Ym-1 expression in the ipsilateral hemisphere, and AG490 administration rescued the decreased expression of Ym-1 in ipsilateral brains of the $KRAS^{G13D/-}$ group. These data indicate that STAT3 inhibition modulates macrophage/microglia polarization in ipsilateral hemisphere and represses neuroinflammation.

3.6. Stroke onset within 3 months after cancer diagnosis was associated with worse prognosis

To examine the relationship between cancer and stroke in patients, we used a hospital-based cancer registry that contained clinical data of all patients diagnosed with colorectal cancer at Osaka University Hospital. From 1 January 2007 to 31 December 2020, 2933 patients with colorectal cancer were included, among which 20 patients developed stroke after admission to the hospital, while 2913 had no stroke onset during follow-up. Baseline characteristics are shown in Table 1. Compared with the group without stroke, cancer patients with stroke onset tended to have higher D-dimer levels ($P = 0.001$), but no statistical differences in CRP ($P = 0.05$), CEA ($P = 0.19$), CA19–9 ($P = 0.38$), or NLR ($P = 0.65$) were found at the timepoint of cancer diagnosis. Nine patients in the stroke group ($n = 20$) who had stroke onset within 3 months after cancer diagnosis were followed up, as 11 patients died within 3 months or had stroke onset after 3 months of cancer diagnosis. In the group without stroke ($n = 2913$), 2702 patients were followed up, as 211 died within 3 months of cancer diagnosis (Fig. 6a). The Kaplan–Meier curve indicated that colorectal cancer patients who had stroke onset within 3 months of cancer diagnosis had poorer prognosis than colorectal cancer patients without stroke development (log-rank test; $P = 0.028$) (Fig. 6b). Overall, our study showed that there is synergistic exacerbation between cancer and stroke that results in worse prognoses. The oncogene *KRAS* may be a potential target of novel treatment for cancer-associated stroke (Fig. 7).

Table 1
Characteristics and outcomes of cancer patients with or without stroke.

Characteristics	Without stroke (n = 2913)	With stroke ($n = 20$)	P value
Age, years (IQR)	66 (57–74)	71 (67–78)	0.04
Female, % (n)	43 (1257)	50 (10)	0.54
BMI, kg/m^2 (IQR)	23 (20–25)	21 (19–25)	0.37
Hypertension, % (n)	31 (910)	55 (11)	0.02
Dyslipidemia, % (n)	21 (598)	40 (18)	0.03
Diabetes mellitus, % (n)	11 (324)	10 (2)	0.87
Atrial fibrillation, % (n)	6 (187)	35 (7)	<0.001
Current smoking, % (n)	15 (440)	20 (4)	0.54
Cancer stage, % (n)			0.16
0	6 (183)	0 (0)	
I	29 (849)	25 (5)	
II	16 (460)	25 (5)	
III	14 (397)	10 (2)	
IV	13 (392)	30 (6)	
Unknown	22 (632)	10 (2)	
Treatment in 5 years after cancer diagnosis*			
Cancer surgery, % (n)	69 (2010)	70 (14)	0.92
Chemotherapy, % (n)	35 (1014)	45 (9)	0.34
Radiation, % (n)	1 (30)	0 (0)	0.65
Anti-thrombotic use, % (n)	25 (729)	40 (8)	0.12
Blood biochemistry in 1 month after cancer diagnosis**			
D-dimer, μg/mL (IQR)	0.49 (0.27–1.02)	1.65 (0.67–2.76)	0.001
CRP, mg/dL (IQR)	0.09 (0.04–0.40)	0.21 (0.07–2.01)	0.05
CEA, ng/mL (IQR)	3.0 (2.0–8.0)	4.0 (3.2–13.5)	0.19
CA19–9, U/mL (IQR)	17.0 (9.9–37.0)	24.4 (13.0–49.6)	0.38
NLR, (IQR)	2.4 (1.8–3.6)	2.7 (1.8–4.0)	0.65

Notes: BMI, body mass index; CRP, C-reactive protein; CEA, carcinoembryonic antigen; CA19-9, carbohydrate antigen 19-9; NLR, neutrophil/lymphocyte ratio.
* The amount of chemotherapy, anticancer surgery, radiotherapy, and antithrombotics are presented until the onset of stroke.
** For patients with stroke, blood biochemistry data before stroke onset were used.

4. Discussion

In this study, we found: (1) Colorectal cancer and stroke interact mutually and aggravated each other, (2) $KRAS^{G13D}$-mutant colorectal cancer triggered STAT3 activation in the brain that promoted neuroinflammation by mediating microglia/macrophages polarization after ischemic stroke, (3) STAT3 inhibition attenuated ischemic stroke outcomes by suppressing neuroinflammation and attenuating p44/42 MAPK pathway inhibition after stroke.

Cancer is an established contributor to thromboembolism [44], and

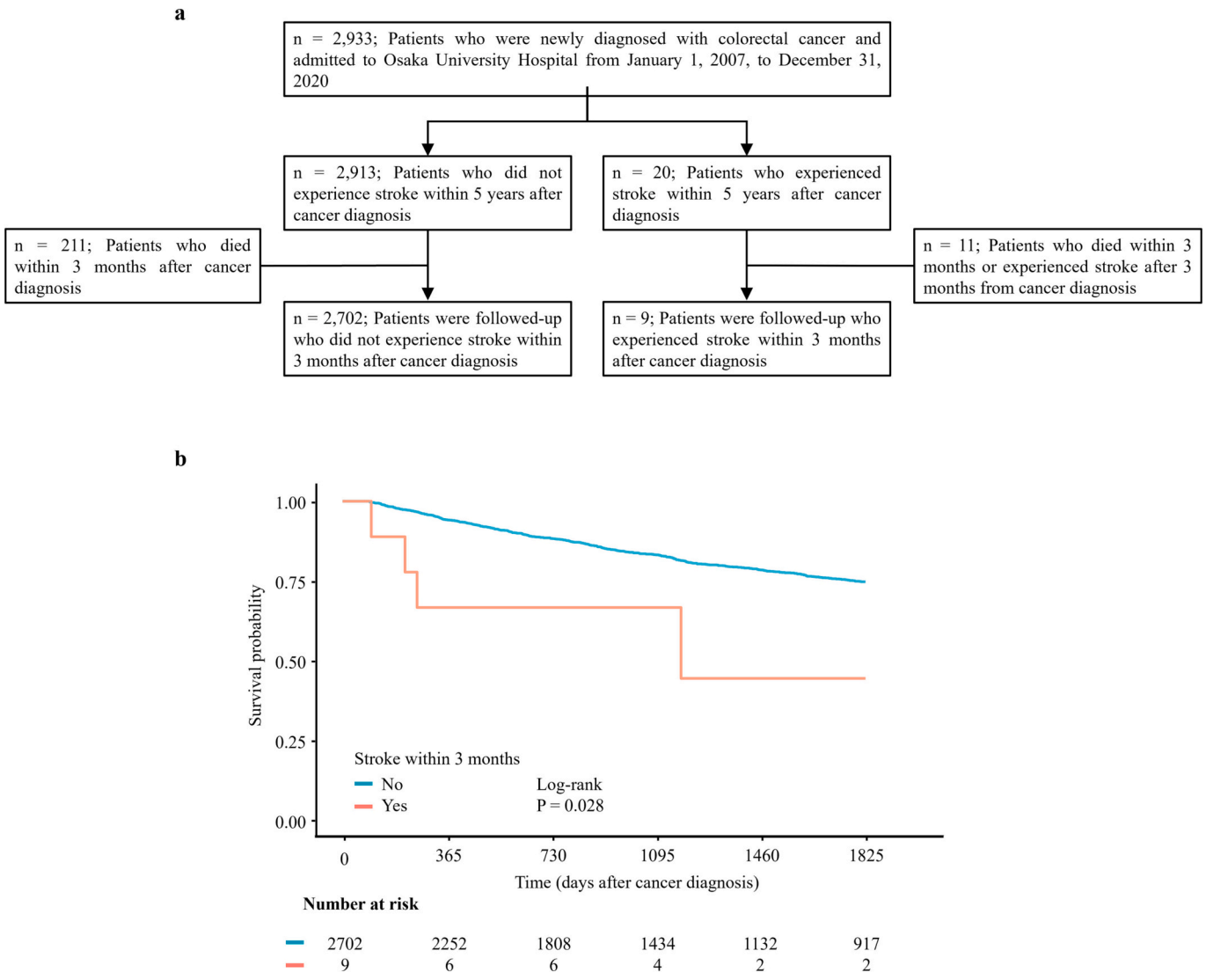

Fig. 6. Kaplan–Meier survival analysis of colorectal cancer patients with or without stroke development within 3 months of cancer diagnosis. a. The inclusion and exclusion criteria for this study. b. Kaplan–Meier survival curve of colorectal cancer patients with or without stroke onset within 3 months of cancer diagnosis.

patients with cancer-associated stroke present higher activation of hypercoagulability, endothelial dysfunction, and more circulating microemboli [45]. Recently, the identification of driver genes has renewed interest in the treatment of cancer-associated stroke. Tumor genomic therapies that target agnostic mutations beyond cancer framework have raised increasing interest in clinical studies [46]. However, little is known about the effects of mutant *KRAS* on the pathology of cancer-associated stroke.

Cancers secrete various cytokines and chemokines into the blood, and thus can interact with distant organs. Among these chemokines, CXCL1 is a well-known biomarker of colorectal cancer [47]. Serum CXCL1 levels are positively correlated with RAS/RAF mutational status in colon cancer patients [48]. Furthermore, CXCL1 has a proinflammatory role in the central nervous system [49], and targeting CXCL1 has been proven to be a promising therapeutic strategy for acute ischemic stroke [50,51]. Interestingly, we found that $KRAS^{G13D}$-mutant cancer induced an elevation of serum CXCL1 levels compared with the parental cell line, which may provide evidence for aggravated neuroinflammatory responses in mice inoculated with $KRAS^{G13D/-}$ HCT116 cells. The potential therapeutic role of CXCL1 in KRAS-driven cancer-associated stroke deserves further experiments.

Among all cytokines, IL-6 exerts a proinflammatory role in systematic diseases and induces STAT3 activation. Targeting STAT3 can be effective in various cancers [52]. But in ischemic stroke, STAT3 has been reported to have dual roles. STAT3 activation alleviates white matter damage [53] but also contributes to neuron damage [54]. Inhibiting STAT3 attenuated infarct volume in mice by suppressing NK cell infiltration [55], mitigating blood brain barrier breakdown [56], and modulating astrocyte differentiation [57]. STAT3 is a classical inducible factor for M2-like macrophages/microglia polarization in tumors [58,59]. However, the role of STAT3 in macrophages/microglia recruitment during thrombotic associated stroke remains unknown. In this study, we found that STAT3 correlates with peri-thrombotic macrophages/microglia accumulation and that inhibiting STAT3 correlates with M2-like macrophages/microglia differentiation in the peri-thrombotic area, suggesting an anti-inflammatory role for STAT3 in thrombotic stroke.

Cancer and stroke mutually interact to aggravate each other, but the mechanism remains elusive due to the intricacies of the involved signaling networks. The roles of macrophages polarization [60], p44/42 MAPK pathway [61] activation, and angiogenesis [62] are opposite in cancer progression and stroke recovery. In this study, we investigated a stroke occurrence and prognosis in colorectal cancer patients using a landmark analysis. Out of the 2711 subjects included in the study, only

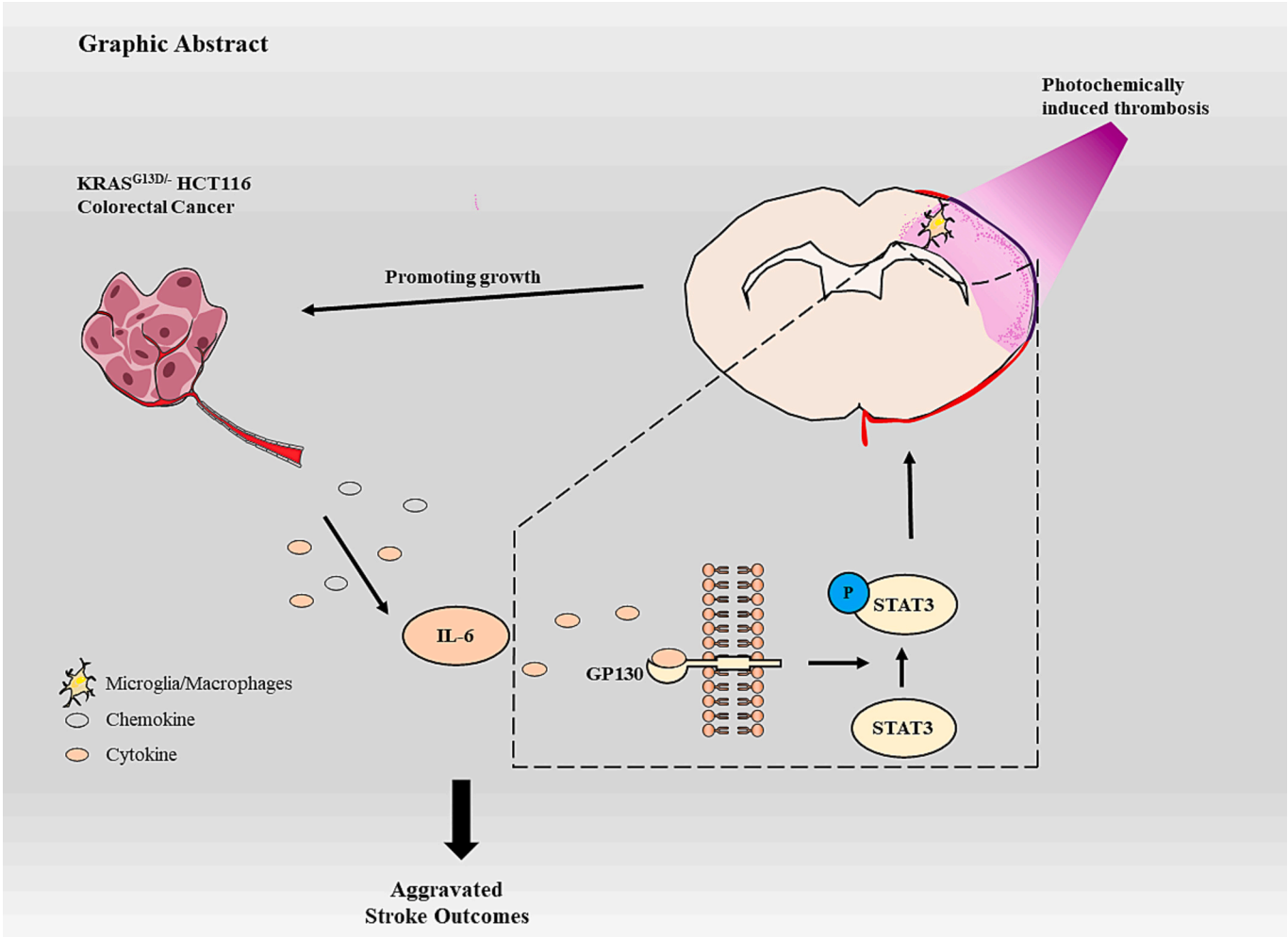

Fig. 7. Graphical abstract. Oncogenic *KRAS*^{G13D} worsened stroke outcomes in HCT116 xenograft-bearing mice by promoting neuroinflammation and tumor growth after experimental stroke.

366 patients were examined for Ras gene mutations. Among the patients who experienced a stroke, only 2 were tested, and none had mutations. On the other hand, among the patients who did not experience a stroke, 364 were examined, and 171 tested positive for mutations. Further researches including multicenter observational study with larger population are needed to clarify the interactions between Ras gene mutations and cancer-associated stroke mortality. Taken together, in this study, we demonstrated that cancer-associated stroke exacerbates ischemic pathology and prognosis both in patients and murine models. Besides, the xenograft experiments indicated that stroke significantly increased tumor size. Stroke-induced immunosuppression and growth factor expression, such as VEGF, may contribute to tumor growth. The mechanism of how stroke induced a rapid increase in tumor size deserves further study, especially for the relationship between stroke and the tumor microenvironment. Taken together, this work may offer a novel insight into the future development of treatments for cancer-associated stroke.

Supplementary data to this article can be found online at https://doi.org/10.1016/j.thromres.2023.11.015.

Declaration of competing interest

The authors declare no conflicts of interest.

Data availability

Raw fastq files for each animal sample were uploaded to the NCBI Gene Expression Omnibus database (GSE223047). All software and code used in this study are described in the Methods. The datasets generated and analyzed during this study are available from the corresponding author upon reasonable request.

Acknowledgements

Not applicable.

CRediT authorship contribution statement

H.Y., T.S., and H.M. designed the experiments. H.Y., H.K., K.N., and T.S. performed the animal experiments. H.Y. and T.S. conducted the RNA-seq data analysis. Y.G. conducted the clinical data analysis. H.Y. and T.S. drafted the manuscript. Critical revisions of the manuscript were made by all authors.

Sources of funding

This work was partially supported by the following grants: Grant-in-Aid for Scientific Research (21K15695; H.K.) (16K15317; T.S.) from the "Ministry of Education, Culture, Sports, Science and Technology – Japan", and the Smoking Research Foundation (H.K. and T.S.).

References

[1] B.B. Navi, C. Iadecola, Ischemic stroke in cancer patients: a review of an underappreciated pathology, Ann. Neurol. 83 (5) (2018) 873–883.
[2] O.Y. Bang, J.W. Chung, M.J. Lee, W.K. Seo, G.M. Kim, M.J. Ahn, et al., Cancer-related stroke: an emerging subtype of ischemic stroke with unique pathomechanisms, J. Stroke 22 (1) (2020) 1–10.
[3] J. Ha, M.J. Lee, S.J. Kim, B.Y. Park, H. Park, S. Cho, et al., Prevalence and impact of venous and arterial thromboembolism in patients with embolic stroke of undetermined source with or without active cancer, J. Am. Heart Assoc. 8 (21) (2019), e013215.
[4] M. Giustozzi, G. Agnelli, J. Del Toro-Cervera, F.A. Klok, R.P. Rosovsky, A.C. Martin, et al., Direct oral anticoagulants for the treatment of acute venous thromboembolism associated with cancer: a systematic review and meta-analysis, Thromb. Haemost. 120 (7) (2020) 1128–1136.
[5] F. Graus, L.R. Rogers, J.B. Posner, Cerebrovascular complications in patients with cancer, Medicine (Baltimore) 64 (1) (1985) 16–35.
[6] D.M. Cestari, D.M. Weine, K.S. Panageas, A.Z. Segal, L.M. DeAngelis, Stroke in patients with cancer: incidence and etiology, Neurology 62 (11) (2004) 2025–2030.
[7] B.B. Navi, A.S. Reiner, H. Kamel, C. Iadecola, M.S. Elkind, K.S. Panageas, et al., Association between incident cancer and subsequent stroke, Ann. Neurol. 77 (2) (2015) 291–300.
[8] B.B. Navi, A.S. Reiner, H. Kamel, C. Iadecola, P.M. Okin, M.S.V. Elkind, et al., Risk of arterial thromboembolism in patients with cancer, J. Am. Coll. Cardiol. 70 (8) (2017) 926–938.
[9] S. Jeong, G. Lee, S. Choi, K.H. Kim, J. Chang, S.M. Kim, et al., Estimating risk of cardiovascular disease among long-term colorectal cancer survivors: a nationwide cohort study, Front. Cardiovasc. Med. 8 (2021), 721107.
[10] J.M. Garcia-Torrecillas, M.C. Olvera-Porcel, M. Ferrer-Marquez, C. Rosa-Garrido, M. Rodriguez-Barranco, M.C. Lea-Pereira, et al., Predictive model of the risk of in-hospital mortality in colorectal cancer surgery, based on the minimum basic data set, Int. J. Environ. Res. Public Health 17 (12) (2020).
[11] A.A. Khorana, C.W. Francis, E. Culakova, N.M. Kuderer, G.H. Lyman, Thromboembolism is a leading cause of death in cancer patients receiving outpatient chemotherapy, J. Thromb. Haemost. 5 (3) (2007) 632–634.
[12] C. Becattini, M. Verso, A. Munoz, G. Agnelli, Updated meta-analysis on prevention of venous thromboembolism in ambulatory cancer patients, Haematologica 105 (3) (2020) 838–848.
[13] Y. Gon, L. Zha, T. Sasaki, T. Morishima, Y. Ohno, H. Mochizuki, et al., Stroke mortality in cancer survivors: a population-based study in Japan, Thromb. Res. 222 (2023) 140–148.
[14] Y. Gon, S. Okazaki, Y. Terasaki, T. Sasaki, T. Yoshimine, M. Sakaguchi, et al., Characteristics of cryptogenic stroke in cancer patients, Ann. Clin. Transl. Neurol. 3 (4) (2016) 280–287.
[15] Y. Gon, D. Kabata, T. Kawano, H. Kanki, K. Todo, T. Sasaki, et al., Hematological abnormalities and malnutrition mediate pathway between cancer and outcomes in ischemic stroke patients, J. Stroke Cerebrovasc. Dis. 29 (8) (2020), 104943.
[16] T. Kawano, T. Sasaki, Y. Gon, T. Kitano, H. Kanki, K. Todo, et al., High neutrophil/lymphocyte ratio at cancer diagnosis predicts incidence of stroke in cancer patients, Brain Commun. 3 (2) (2021), fcab071.
[17] T. Kitano, T. Sasaki, Y. Gon, K. Todo, S. Okazaki, T. Kitamura, et al., The effect of chemotherapy on stroke risk in cancer patients, Thromb. Haemost. 120 (4) (2020) 714–723.
[18] M.E. Salem, S.M. El-Refai, W. Sha, A. Puccini, A. Grothey, T.J. George, et al., Landscape of KRAS(G12C), associated genomic alterations, and interrelation with immuno-oncology biomarkers in KRAS-mutated cancers, JCO Precis. Oncol. 6 (2022), e2100245.
[19] R. Thangaiyan, I.A. Aljahdali, K.Y. Lent-Moore, J. Liao, X. Ling, F. Li, Kras mutation subtypes distinctly affect colorectal cancer cell sensitivity to FL118, a novel inhibitor of survivin, Mcl-1, XIAP, cIAP2 and MdmX, Am. J. Transl. Res. 13 (7) (2021) 7458–7474.
[20] B. Grabner, D. Schramek, K.M. Mueller, H.P. Moll, J. Svinka, T. Hoffmann, et al., Disruption of STAT3 signalling promotes KRAS-induced lung tumorigenesis, Nat. Commun. 6 (2015) 6285.
[21] Z.B. Jiang, W.J. Wang, C. Xu, Y.J. Xie, X.R. Wang, Y.Z. Zhang, et al., Luteolin and its derivative apigenin suppress the inducible PD-L1 expression to improve anti-tumor immunity in KRAS-mutant lung cancer, Cancer Lett. 515 (2021) 36–48.
[22] B.R. Sharma, R. Karki, B. Sundaram, Y. Wang, P. Vogel, T.D. Kanneganti, The transcription factor IRF9 promotes colorectal cancer via modulating the IL-6/STAT3 signaling axis, Cancers (Basel) 14 (4) (2022).
[23] J. Korac-Prlic, M. Degoricija, K. Vilovic, B. Haupt, T. Ivanisevic, L. Frankovic, et al., Targeting Stat3 signaling impairs the progression of bladder cancer in a mouse model, Cancer Lett. 490 (2020) 89–99.
[24] C. Won, B.H. Kim, E.H. Yi, K.J. Choi, E.K. Kim, J.M. Jeong, et al., Signal transducer and activator of transcription 3-mediated CD133 up-regulation contributes to promotion of hepatocellular carcinoma, Hepatology 62 (4) (2015) 1160–1173.
[25] X. Yang, Q. Yv, F. Ye, S. Chen, Z. He, W. Li, et al., Echinacoside protects dopaminergic neurons through regulating IL-6/JAK2/STAT3 pathway in Parkinson's disease model, Front. Pharmacol. 13 (2022), 848813.
[26] Z. Dong, X. Liang, Q. Zhang, S. Luo, H. Liu, X. Wang, et al., Folic acid deficiency enhances the Tyr705 and Ser727 phosphorylation of mitochondrial STAT3 in in vivo and in vitro models of ischemic stroke, Transl. Stroke Res. 12 (5) (2021) 829–843.
[27] Z.V. Zheng, J. Chen, H. Lyu, S.Y.E. Lam, G. Lu, W.Y. Chan, et al., Novel role of STAT3 in microglia-dependent neuroinflammation after experimental subarachnoid haemorrhage, Stroke Vasc. Neurol. 7 (1) (2022) 62–70.
[28] L. Abjean, L. Ben Haim, M. Riquelme-Perez, P. Gipchtein, C. Derbois, M. A. Palomares, et al., Reactive astrocytes promote proteostasis in Huntington's disease through the JAK2-STAT3 pathway, Brain 146 (1) (2023 Jan 5) 149–166.
[29] H. Zhu, Z. Jian, Y. Zhong, Y. Ye, Y. Zhang, X. Hu, et al., Janus kinase inhibition ameliorates ischemic stroke injury and neuroinflammation through reducing NLRP3 inflammasome activation via JAK2/STAT3 pathway inhibition, Front. Immunol. 12 (2021), 714943.
[30] R. Wang, S. Zhang, Z. Yang, Y. Zheng, F. Yan, Z. Tao, et al., Mutant erythropoietin enhances white matter repair via the JAK2/STAT3 and C/EBPbeta pathway in middle-aged mice following cerebral ischemia and reperfusion, Exp. Neurol. 337 (2021), 113553.
[31] H. Yan, T. Sasaki, H. Kanki, Y. Hirata, K. Nishiyama, S. Hisada, et al., MDMX elevation by a novel Mdmx-p53 interaction inhibitor mitigates neuronal damage after ischemic stroke, Sci. Rep. 12 (1) (2022) 21110.
[32] H. Yan, H. Kanki, S. Matsumura, T. Kawano, K. Nishiyama, S. Sugiyama, et al., MiRNA-132/212 regulates tight junction stabilization in blood-brain barrier after stroke, Cell Death Discov. 7 (1) (2021) 380.
[33] Y. Gon, D. Kabata, K. Yamamoto, A. Shintani, K. Todo, H. Mochizuki, et al., Validation of an algorithm that determines stroke diagnostic code accuracy in a Japanese hospital-based cancer registry using electronic medical records, BMC Med. Inform. Decis. Mak. 17 (1) (2017) 157.
[34] Y. Gon, T. Sasaki, T. Kawano, S. Okazaki, K. Todo, T. Takeda, et al., Impact of stroke on survival in patients with cancer, Thromb. Res. 222 (2023) 109–112.
[35] S. Grazioli, M. Paciaroni, G. Agnelli, M. Acciarresi, A. Alberti, C. D'Amore, et al., Cancer-associated ischemic stroke: a retrospective multicentre cohort study, Thromb. Res. 165 (2018) 33–37.
[36] M. Woock, N. Martinez-Majander, D.J. Seiffge, H.A. Selvik, A. Nordanstig, P. Redfors, et al., Cancer and stroke: commonly encountered by clinicians, but little evidence to guide clinical approach, Ther. Adv. Neurol. Disord. 15 (2022), 17562864221106362.
[37] N. Wang, W. Liu, Y. Zheng, S. Wang, B. Yang, M. Li, et al., CXCL1 derived from tumor-associated macrophages promotes breast cancer metastasis via activating NF-kappaB/SOX4 signaling, Cell Death Dis. 9 (9) (2018) 880.
[38] Z.J. Zhang, B.C. Jiang, Y.J. Gao, Chemokines in neuron-glial cell interaction and pathogenesis of neuropathic pain, Cell. Mol. Life Sci. 74 (18) (2017) 3275–3291.
[39] M. Amin, A. Vakilian, M.H. Mahmoodi, G. Hassanshahi, S.K. Falahati-Pour, M. R. Dolatabadi, et al., Circulatory levels of C-X-C motif chemokine ligands 1, 9, and 10 are elevated in patients with ischemic stroke, Eurasian J. Med. 49 (2) (2017) 92–96.
[40] S. Suzuki, K. Tanaka, N. Suzuki, Ambivalent aspects of interleukin-6 in cerebral ischemia: inflammatory versus neurotrophic aspects, J. Cereb. Blood Flow Metab. 29 (3) (2009) 464–479.
[41] E. Cheng, Q. Shi, A.F. Shields, A.B. Nixon, A.P. Shergill, C. Ma, et al., Association of inflammatory biomarkers with survival among patients with stage III colon cancer, JAMA Oncol. 9 (3) (2023 Mar 1) 404–413.
[42] X. Hu, P. Li, Y. Guo, H. Wang, R.K. Leak, S. Chen, et al., Microglia/macrophage polarization dynamics reveal novel mechanism of injury expansion after focal cerebral ischemia, Stroke 43 (11) (2012) 3063–3070.
[43] M. Kanazawa, I. Ninomiya, M. Hatakeyama, T. Takahashi, T. Shimohata, Microglia and monocytes/macrophages polarization reveal novel therapeutic mechanism against stroke, Int. J. Mol. Sci. 18 (10) (2017).
[44] S.M. Silvis, S. Hiltunen, E. Lindgren, K. Jood, S.M. Zuurbier, S. Middeldorp, et al., Cancer and risk of cerebral venous thrombosis: a case-control study, J. Thromb. Haemost. 16 (1) (2018) 90–95.
[45] B.B. Navi, C.P. Sherman, R. Genova, R. Mathias, K.N. Lansdale, N.M. LeMoss, et al., Mechanisms of ischemic stroke in patients with cancer: a prospective study, Ann. Neurol. 90 (1) (2021) 159–169.
[46] M.R. Waarts, A.J. Stonestrom, Y.C. Park, R.L. Levine, Targeting mutations in cancer, J. Clin. Invest. 132 (8) (2022).
[47] L. Yu, X. Yang, C. Xu, J. Sun, Z. Fang, H. Pan, et al., Comprehensive analysis of the expression and prognostic value of CXC chemokines in colorectal cancer, Int. Immunopharmacol. 89 (Pt B) (2020), 107077.
[48] Y.L. Park, H.P. Kim, C.Y. Ock, D.W. Min, J.K. Kang, Y.J. Lim, et al., EMT-mediated regulation of CXCL1/5 for resistance to anti-EGFR therapy in colorectal cancer, Oncogene 41 (14) (2022) 2026–2038.
[49] B.D. Michael, L. Bricio-Moreno, E.W. Sorensen, Y. Miyabe, J. Lian, T. Solomon, et al., Astrocyte- and neuron-derived CXCL1 drives neutrophil transmigration and blood-brain barrier permeability in viral encephalitis, Cell Rep. 32 (11) (2020), 108150.
[50] D. Li, W. Lang, C. Zhou, C. Wu, F. Zhang, Q. Liu, et al., Upregulation of microglial ZEB1 ameliorates brain damage after acute ischemic stroke, Cell Rep. 22 (13) (2018) 3574–3586.
[51] S.M. Stamatovic, C.M. Phillips, R.F. Keep, A.V. Andjelkovic, A novel approach to treatment of thromboembolic stroke in mice: redirecting neutrophils toward a peripherally implanted CXCL1-soaked sponge, Exp. Neurol. 330 (2020), 113336.
[52] P.S. Thilakasiri, R.S. Dmello, T.L. Nero, M.W. Parker, M. Ernst, A.L. Chand, Repurposing of drugs as STAT3 inhibitors for cancer therapy, Semin. Cancer Biol. 68 (2021) 31–46.
[53] C. Qin, W.H. Fan, Q. Liu, K. Shang, M. Murugan, L.J. Wu, et al., Fingolimod protects against ischemic white matter damage by modulating microglia toward M2 polarization via STAT3 pathway, Stroke 48 (12) (2017) 3336–3346.

[54] I. Satriotomo, K.K. Bowen, R. Vemuganti, JAK2 and STAT3 activation contributes to neuronal damage following transient focal cerebral ischemia, J. Neurochem. 98 (5) (2006) 1353–1368.
[55] S. Li, B. Dou, S. Shu, L. Wei, S. Zhu, Z. Ke, et al., Suppressing NK cells by astragaloside IV protects against acute ischemic stroke in mice via inhibiting STAT3, Front. Pharmacol. 12 (2021), 802047.
[56] S.Y. Xu, H.J. Bian, S. Shu, S.N. Xia, Y. Gu, M.J. Zhang, et al., AIM2 deletion enhances blood-brain barrier integrity in experimental ischemic stroke, CNS Neurosci. Ther. 27 (10) (2021) 1224–1237.
[57] X. Cheng, P.K.K. Yeung, K. Zhong, P.L.M. Zilundu, L. Zhou, S.K. Chung, Astrocytic endothelin-1 overexpression promotes neural progenitor cells proliferation and differentiation into astrocytes via the Jak2/Stat3 pathway after stroke, J. Neuroinflammation 16 (1) (2019) 227.
[58] M. Qian, S. Wang, X. Guo, J. Wang, Z. Zhang, W. Qiu, et al., Hypoxic glioma-derived exosomes deliver microRNA-1246 to induce M2 macrophage polarization by targeting TERF2IP via the STAT3 and NF-kappaB pathways, Oncogene 39 (2) (2020) 428–442.
[59] D. Ma, S. Liu, B. Lal, S. Wei, S. Wang, D. Zhan, et al., Extracellular matrix protein tenascin C increases phagocytosis mediated by CD47 loss of function in glioblastoma, Cancer Res. 79 (10) (2019) 2697–2708.
[60] A. Mantovani, P. Allavena, F. Marchesi, C. Garlanda, Macrophages as tools and targets in cancer therapy, Nat. Rev. Drug Discov. 21 (11) (2022) 799–820.
[61] J. Urosevic, M.T. Blasco, A. Llorente, A. Bellmunt, A. Berenguer-Llergo, M. Guiu, et al., ERK1/2 signaling induces upregulation of ANGPT2 and CXCR4 to mediate liver metastasis in colon cancer, Cancer Res. 80 (21) (2020) 4668–4680.
[62] Y. Yang, Y. Cao, The impact of VEGF on cancer metastasis and systemic disease, Semin. Cancer Biol. 86 (2022) 251–261.